



Numerical study of eddy current by Finite Element Method for cracks detection in structures

S. Harzallah, M. Chabaat, K. Chabane

University Built Environmental Research Lab., Civil Engineering Faculty, University of Sciences and Technology Houari Boumediene, B.P 32 El Alia Bab Ezzouar, Algiers 16111 Algeria.
sharzallah@usthb.dz, M.Chabaat@usthb.dz, Kabinachabane91@yahoo.fr

ABSTRACT. In this paper, we try to use the finite element method of 2-D axisymmetry to solve problems in eddy current testing problems where the main idea is detecting crack's shape using the NDT-EC. Results are given for a simple eddy current problem using the finite element method as a tool to control cracks and defects in materials and eventually, to study their propagation as well as their shape classification. These latest can be described as the task of reconstructing the cracks and damage in a tube's profile of an inspected specimen in order to estimate its material properties. This is accomplished by inverting eddy current probe impedance measurements which are recorded as a function of probe position. This approach has been used in the aircraft industry to control cracks. Besides, it makes it possible to highlight the defects of parts while preserving the integrity of the controlled products.

KEYWORDS. Non destructive testing; Sensor eddy currents; Differential mode; Stress intensity factor.



Citation: Harzallah, S., Chabaat, M., Chabane, K., Numerical study of eddy current by Finite element method for cracks detection in structures, *Frattura ed Integrità Strutturale*, 39 (2017) 282-290.

Received: 13.10.2016

Accepted: 09.12.2016

Published: 01.01.2017

Copyright: © 2017 This is an open access article under the terms of the CC-BY 4.0, which permits unrestricted use, distribution, and reproduction in any medium, provided the original author and source are credited.

INTRODUCTION

There are often sharp breaks that cause bad consequences because of existing defects (cracks, micro-cracks, crazes etc...) inside or outside parts [1]. On the other hand, usual calculations of continuum mechanics cannot predict fracture because it requires the absence of any failure or the development of fracture mechanics, defined as the science studying a structure with defects [2]. It is characterized by irreversible separation of a continuous medium into two parts on either side of a geometrical surface called crack created by damage under the effect of a biasing or default prepared when setting. It also controls the evolution of the crack, [3].

In the aircraft industry as well as in the majority of industries of transport, the non-destructive tests (NDT) can make the difference between life and death. Non-destructive examination using inductive sensors is a relatively common method in the industry (aviation, automotive, nuclear power, etc...). Its development is primarily due to the advanced technology provided. The NDT aims to detect cracks while preserving the integrity of the product. This definition is rather broad and



related particularly to the health of the matter [1, 2]. The non-destructive testing of materials became a tool impossible to circumvent for the improvement of safety (at the time of the uniform), and of quality (during the development) [3]. Eddy current sensor devices have been used for over a century in the control of conductive parts including metal parts. Nowadays, the theory of Eddy current sensors is already largely developed. We find its applications in various industrial fields, ranging from the measurement of the properties of matter to the detection of flaws in metal parts. Due to their sensitivity to defects (fatigue cracks, inclusions or corrosion effects) [4] their implementation, easy and robust, is widespread in the context of industrial use. However, the growing need for reliability and rapidity of checking operations lead to the development of new sensors [5]. Detection and characterization of a crack in a plate at its initial stage (before propagation), is a real industrial challenge and a major element in safety especially in high-risk areas. It is on the basis of these characterizations that engineers have the means to analyze such crack behavior, predict its spread and eventually assess its harmfulness as well as the life of the inspected body, [6].

In this paper, a numerical model for the assessment of eddy currents in materials, for the detection and characterization of defects is considered. We first describe the physical and geometrical properties of used materials and then, we present, through an example, results of eddy currents obtained using a numerical model that we have developed. The most promising numerical technique for computation of eddy current fields is the FEM. This method has proven usefulness in demonstrating the feasibility of flaw detection under given inspection conditions. The problems studied in this work of this paper are the NDT by EC of ferromagnetic materials. These materials are largely used in various industrial fields, such as aeronautics, metallurgy and rail transport.

BASIC EQUATIONS

Distribution of the magnetic field and the currents induced in a conducting material, and possibly magnetic, is governed by the fundamental laws of the electromagnetism whose most general formulation is given by the Maxwell's equations [7]:

$$\left\{ \begin{array}{l} \nabla \cdot \vec{E} = \frac{\rho}{\epsilon_0} \\ \nabla \cdot \vec{B} = 0 \\ \nabla \times \vec{E} = -\frac{\partial \vec{B}}{\partial t} \\ \nabla \times \vec{B} = \mu_0 \epsilon_0 \frac{\partial \vec{E}}{\partial t} + \mu_0 \vec{J}_s \end{array} \right. \quad (1)$$

where, \vec{B} is the magnetic induction and \vec{E} represents the electrical field.

The quantities ρ and \vec{J}_s are the volume charge density and the electrical current density (flux) of any external charges, respectively.

PROPOSED MODEL

Eddy current testing systems consist of configurations that are present in Fig. 1 such as the conductor sensor in which Ω_c , Ω_{nk} represent the sample conducting region and cracks area (a damage region), respectively. On the other hand, Ω_k refers to the conductor region with its normal vector \vec{n} . In a multi-conductor sensor, a high coupling is considered from the sensor and the tube as a sample. The Primary field resulting from the current source I_k includes contribution to the flow of all conductors Ω_k which interact entirely all due to proximity effect. In another mode, every conductor interacts with the secondary field produced by the eddy current induced in the sample. For the massive conductor ($\bigcup \Omega_k$) and $\sum (I_s)_k$ the interaction from the primary and secondary fields are weak because all considerations on the effects of skin and proximity [8].



Mathematical division may be achieved by the following partial differential equation. The FEM for EC phenomena 2D revolution has been developed in numerous works. For axisymmetric geometries set equations to 2D. We suggest that two-dimensional cylindrical coordinates are considered in order to study these system components of the current density $\bar{J}_s = (0, 0, J_{s\phi}(r, \varphi))$. The Magnetic Vector Potential $\bar{A} = (0, 0, A_\phi(r, \varphi))$ and the two-dimensional cylindrical components of the Magnetic Vector Potential (MVP) diffusion are related as follows;

$$\frac{\partial}{\partial r} \left(\frac{1}{\mu r} \frac{\partial (r A_\phi)}{\partial r} \right) + \frac{\partial}{\partial \varphi} \left(\frac{1}{\mu r} \frac{\partial (r A_\phi)}{\partial \varphi} \right) = \begin{cases} 0 & \text{in } \Omega_{nc} \\ -j\omega \frac{\sigma}{r} (r A_\phi) & \text{in } \Omega_c \\ \frac{\bar{n} \cdot \frac{I_{sk}}{S_k}}{S_k} & \text{in } \Omega_k \\ \sum_{k=1}^{N_{coils}} \frac{\bar{n} \cdot (I_s)_k}{S_k} & \text{in } \cup \Omega_k \end{cases} \quad (2)$$

where, j is the complex number, ω is the angular frequency, I_{sk} , $S_k = \iint_{\Omega_k} ds$ [9]. Applying the Galerkin's method, with approximation functions of the Magnetic Vector Potential (MVP), and using Dirichlet boundary conditions, we can write every mesh nodes into discrete forms as follows;

$$\sum_{j=1}^n \left[\frac{1}{\mu} \iint_{\Omega} \vec{\nabla} N_m \vec{\nabla} N_n d\Omega \right] A_j = \begin{cases} 0 & \text{in } \Omega_{nc} \\ -j\omega \sum_{j=1}^n \left[\iint_{\Omega} \sigma \cdot N_m N_n d\Omega \right] A_j & \text{in } \Omega_c \\ \iint_{\Omega} N_m \bar{n} \cdot \frac{I_{sk}}{S_k} d\Omega_k & \text{in } \Omega_k \\ \sum_{k=1}^{N_{coils}} \iint_{\Omega} N_m \bar{n} \cdot \frac{(I_s)_k}{S_k} d\Omega_k & \text{in } \cup \Omega_k \end{cases} \quad (3)$$

where N_n is the approximation function at node n , N_m is the shape function for all nodes in a given region. Then, we get the following algebraic equations [10]

$$[M] = \begin{cases} 0 & \text{in } \Omega_{nc} \\ -j\omega [K][A] & \text{in } \Omega_c \\ [F] & \text{in } \Omega_k \\ \sum_{k=1}^{N_{coils}} [F] & \text{in } \cup \Omega_k \end{cases} \quad (4)$$

where

$$M_{mn} = \iint_{\Omega} \left[\frac{1}{\mu} \iint_{\Omega} \vec{\nabla} N_m \vec{\nabla} N_n d\Omega \right] d\Omega \quad (5)$$

$$K_{mn} = \iint_{\Omega} \sigma \cdot N_m \cdot N_n d\Omega_k \quad (6)$$

$$F_m = \iint_{\Omega} N_m \bar{n} \cdot \frac{I_{sk}}{S_k} d\Omega_k \quad (7)$$

IMPEDANCE ANALYSIS

Detection of the change in the resulting magnetic fields is based on two basic methods: the NDT differential mode represented by two separate coils linked magnetically and supplied by the same current and the NDE absolute mode which makes use of only one coil. The impedance variation is obtained from comparison with the reference impedance. The impedance variation Z is a complex number. The imaginary part is computed with the magnetic energy (W_M) in the whole meshed domain and the real part is computed with the Joule Losses in the conductive media and the imaginary part is computed with the magnetic energy in the whole meshed domain [11].

The coil impedance with an excited current at a frequency F is obtained by the following expression [12]:

$$\left\{ \begin{array}{l} Re(Z) = \frac{JL}{I^2} \\ Re(\Delta Z) = \int_c \frac{1}{\sigma} \left(|J_f|^2 - |J|^2 \right) d \end{array} \right. \quad (8)$$

and,

$$\left\{ \begin{array}{l} Im(Z) = \frac{\omega W_M}{I^2} \\ Im(\Delta Z) = \omega \int_c \frac{1}{\mu} \left(|B_f|^2 - |B|^2 \right) d \end{array} \right. \quad (9)$$

$$\left\{ \begin{array}{l} Z = R + jX \\ Z = \frac{1}{I^2} \left(\int \frac{J^2}{\sigma} d + j2 \pi F \int (\vec{B} \cdot \vec{H}) d \right) \end{array} \right. \quad (10)$$

where, Z is the impedance given as a complex number, JL represents the Joule Losses and W_M corresponds to the magnetic energy. I is the current source and H is the magnetic field. Besides, J_f , J and B_f , B are the current density field and the magnetic induction field, respectively. These parameters are calculated with and without a defect and are both software post-treatment quantities.

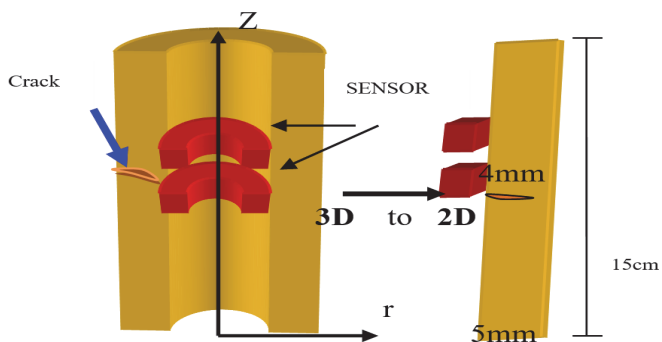


Figure 1: Sensor-Tube geometrical configuration.

SIMULATION SENSOR – TUBE WITHOUT A CRACK

The inspection of tubes is usually carried out by using the eddy currents testing through the analysis of the impedance variations. The considered device is shown in Fig. 1. For the first application, we tested a non-magnetic tube without any crack and characterized by a permeability equal to the unit, a high conductivity $36.7 \cdot 10^6 \text{ ms}$,



excited by a sinusoidal current of density of current $J = 2.67 \times 10^6$ A/m and a frequency of 10 kHz. Here, the crack size length is taken to be 4mm.

Results interpretations

Results of a simulation obtained for the case of a non-magnetic tube without defects are illustrated in the following figures:

Fig. 2 represents the distribution of the potential of the vector. It exposes a great power of concentration of the potential to the level of the inductor and of weak in values from where the high use of the frequency.

Figs. 3 and 4 show the orientation of the field lines. This field concentrates on the level of the probe and its degree penetration depth in the tube remains very weak. Besides, the effect of the penetration depth on a side is crucial for a high frequency and depends on other dimensions as well as the nature of the non-magnetic target representing the homogeneous part.

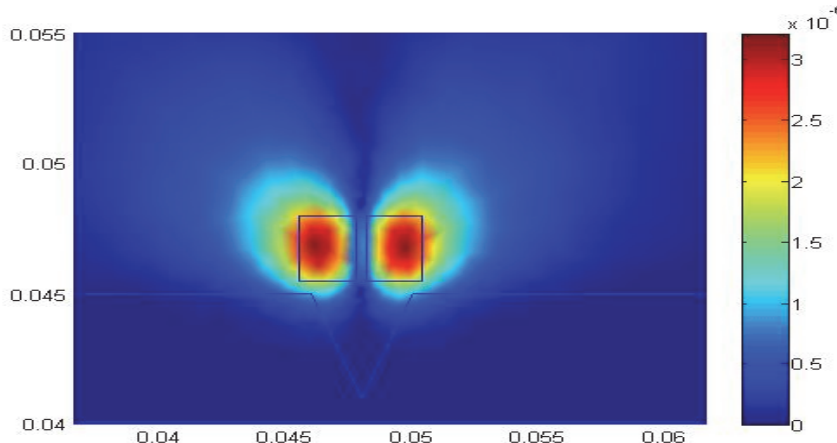


Figure 2: Representation of the potential vector.

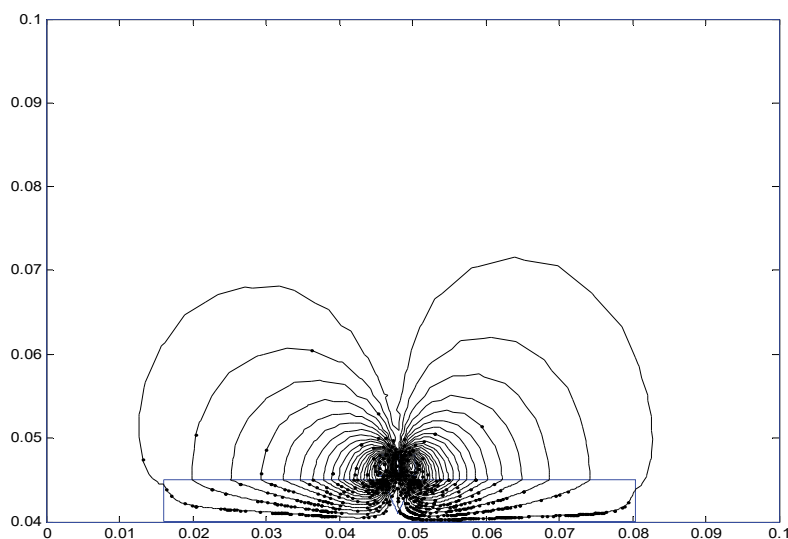


Figure 3: Circulation of the field lines.

Fig. 5 gives lines of equipotential of the real part (the source) and the imaginary part (the part induced in the load) of the magnetic potential vector with a zero value of the magnetic potential on L axis of symmetry of the two reels.

Fig. 6 indicates the distribution of magnetic induction. That explains the strong concentration of the vectors of magnetic induction on the level of the inductor without the possibility to penetrate inside the tube due to the characteristics of the material and the effect of the frequency. It represents the vectors of magnetic inductions which turn around the two inductors in contrary directions because of the reverse excitation of the two inductors.

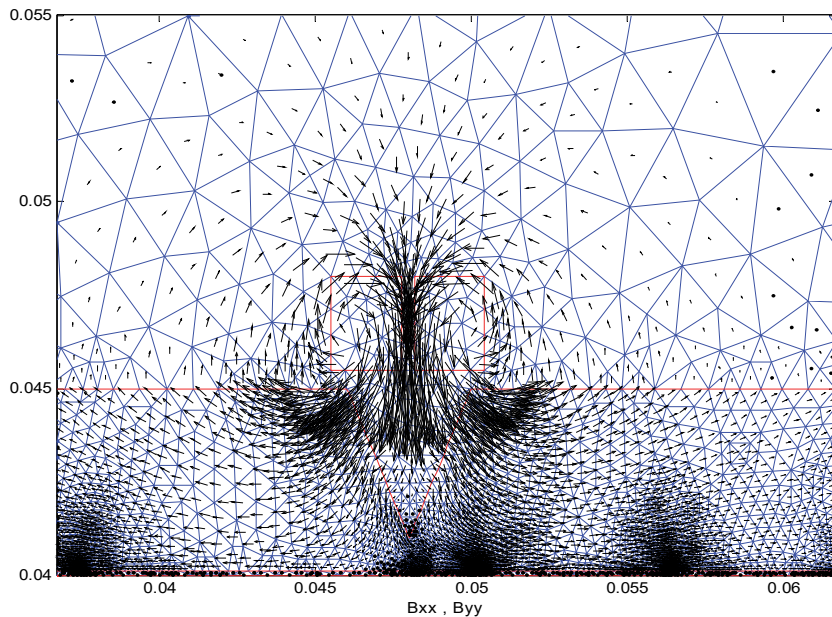


Figure 4: Representation of the vector of induction B.

Fig. 7 represents the distribution of the currents induced on the surface of target. It is noticed that their values are high because the conductivity of the non-magnetic target is considerable ($j = \sigma \cdot 2\pi \cdot f \cdot A$) but are relatively weak compared to the primary currents.

It is known that the complex impedance has two parts, a real part given by resistance and an imaginary part given by the reluctance. In the analysis of Fig. 8, we remark that more the frequency is high and more the impedance Z , given by the difference between the two impedances constituting the sensor, increases. This increase is due to the effect of skin being very important and also, to an existing crack.

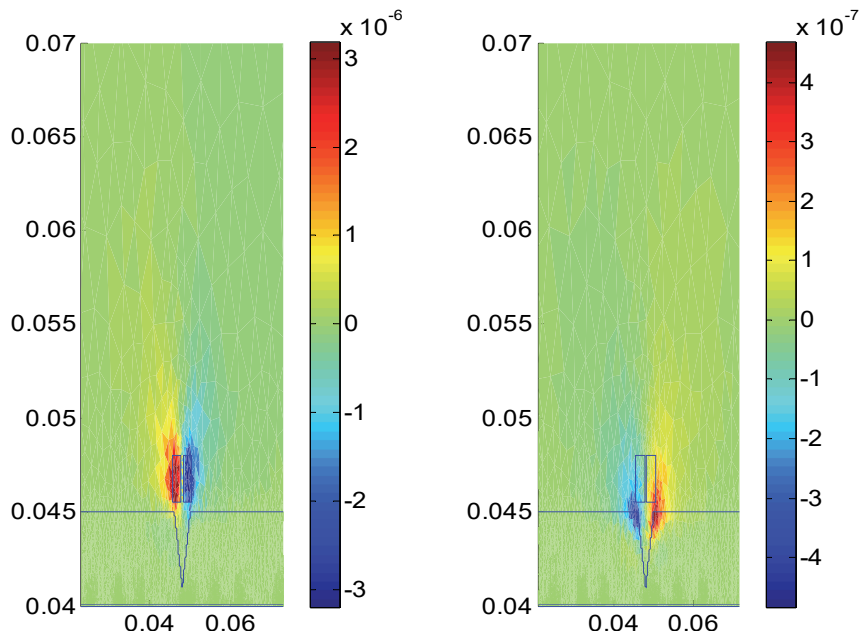


Figure 5: Representation of the real and imaginary part of the potential.

Figs. 9 and 10 represent the evaluation of resistance and reactance of the sensor (Ω).

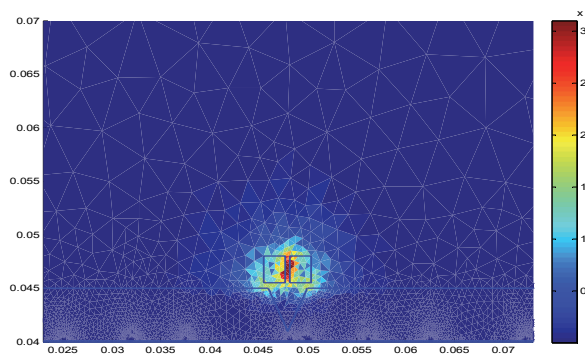


Figure 6: Representation of the magnetic induction.

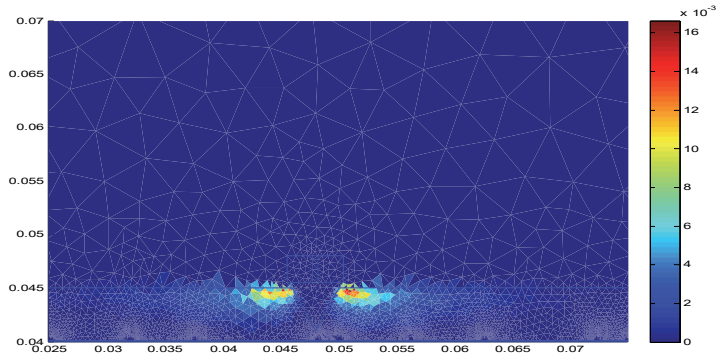
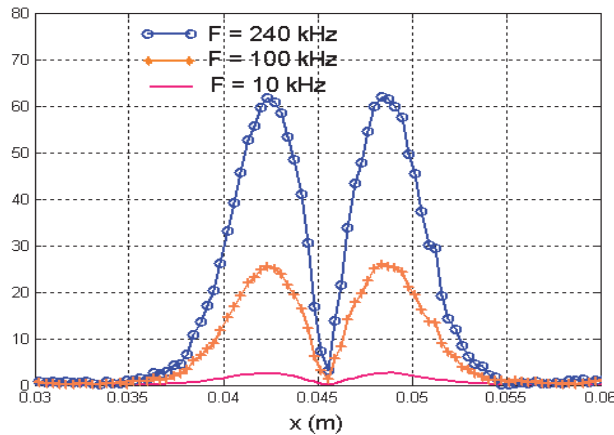
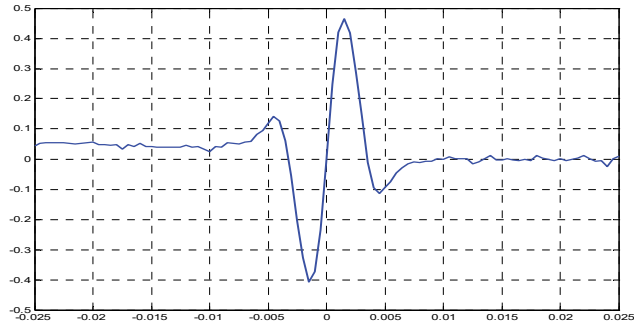
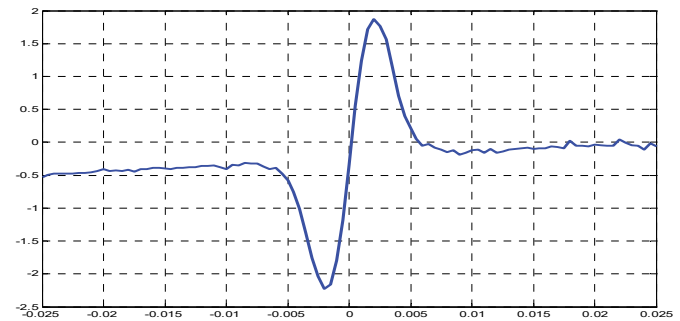


Figure 7: Density of induced currents.

Figure 8: ΔZ for $F = 10, 100$ and 240 KHz.Figure 9: The imaginary part impedance Z (Ω).Figure 10: The real part impedance Z (Ω).

Effects between dimensions of a defect and the sensors

In this research, we consider two cases of shape's geometries. Each one includes three different defects and for each system, we obtain results after the execution of the program. These values are represented in the form of curves of the impedance ΔZ .

In Fig. 11 and 12, when the width decreases, the value of impedance ΔZ decreases. The width of the defect has a great influence on the variation of impedance. The variation depth of the defect has a light influence on ΔZ . It is noticed that the difference of impedance ΔZ has a relationship with the width of the defect. Whenever the width of defect increases, ΔZ automatically increases and vice versa. Consequently, the depth of defect has an influence on impedance. The variation depth of the defect has a light influence on ΔZ . It is noticed that the difference of impedance ΔZ correlates with the width of the defect. It is noticed that the difference of impedance ΔZ has a dependency on the width of the defect and the depth of a defect has a great influence on the impedance.

Figs. 13-16 represent the evaluation of resistance and reactance of the sensor versus the crack depth and width. We notice that when the width decreases, the value of resistance and the reactance decrease in a proportional way.

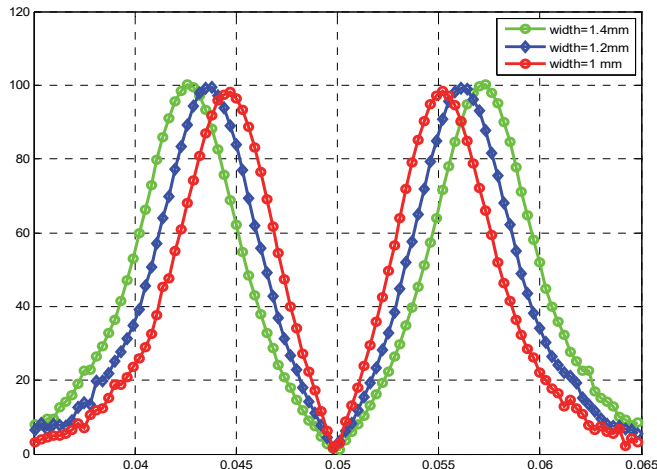


Figure 11: Impedance Z vs. crack width.

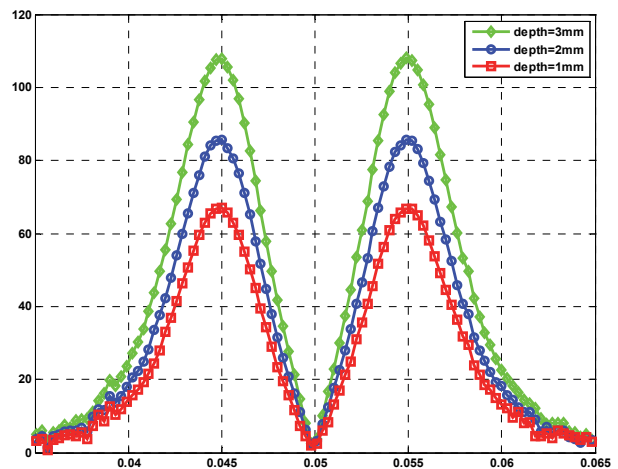


Figure 12: Impedance Z vs. crack depth.

CONCLUSION

It is shown through this research work that obtained results are identified by a variation of impedance of the magnetic currents values. These values agreed with the previous results that lead us to determine the mechanical properties of fracture of materials. The new approach has been useful in the study of expansion and crack propagation in materials. It can easily predict a future damage of mechanical parts. Besides, this technique can be benefit in the treatment of materials rather than changing parts. It gives accurate results and high performance for parts of materials. Herein, a possible prediction of cracks propagation through the determination of parameters SIF and J-integral using eddy current by detecting crack tip opening displacement is described. Similar results are obtained for both parameters K and J-integral using variation of the impedance. Notice that this method is widely used in industrial application because of its precision (minimal error) and its low costs.

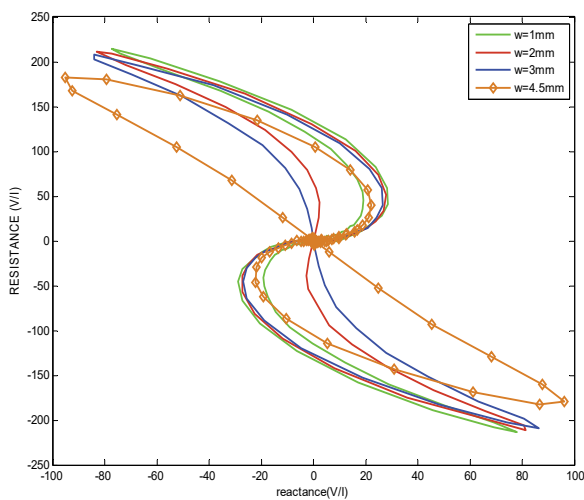


Figure 13: Evaluation of resistance and reactance sensor vs. crack depth.

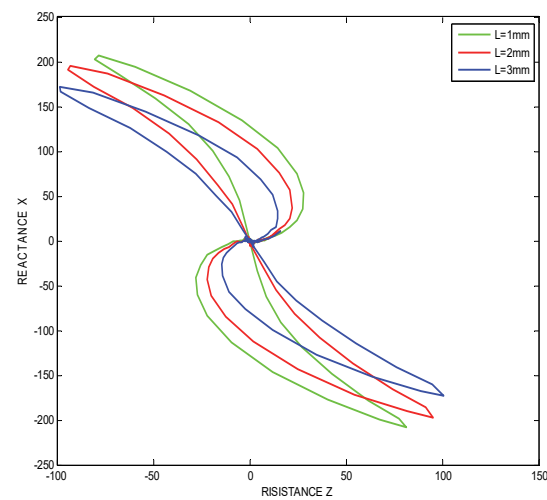


Figure 14: Evaluation of resistance and reactance sensor vs. crack width.

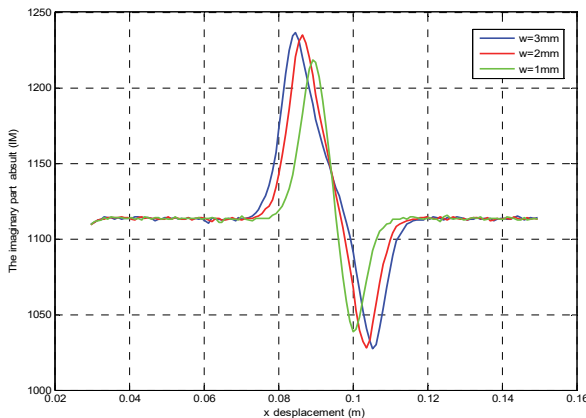


Figure 15: Evaluation of the reactance of the sensor vs. crack width.

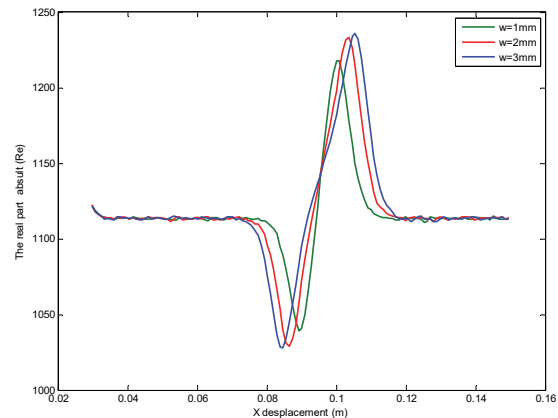


Figure 16: Evaluation of resistance of the sensor vs. crack depth.

REFERENCES

- [1] Horan, P., Underhill, P. R., Krause, T. W., Pulsed eddy current detection of cracks in F/A-18 inner wing spar without wing skin removal using modified principal component analysis, NDT&E International, 55 (2013) 21-27.
- [2] Hamia, R., Dolabdjian, C., Eddy-current non-destructive testing system for the determination of crack orientation, NDT & E International, 61 (2014) 24–28.
- [3] Uchimoto, T., Takagi, T., Ichihara, T., Dobmann, G., Evaluation of fatigue cracks by an angle beam EMAT-ET dual probe, NDT & E International, 72 (2015) 10–16.
- [4] Zaoui, A., Menana, H., Feliachi, M., Berthiau, G., Inverse problem in nondestructive testing using arrayed eddy current sensors. Sensors, 10(9) (2010) 8696-8704.
- [5] Skarlatos, A., Pichenot, G., Lesselier, D., Electromagnetic modeling of a damaged ferromagnetic metal tube via a volume integral formulation, IEEE Trans. Mag, 44 (2008) 623-632.
- [6] Garcia-Martin, J., Gomez-Gil, J., Vazquez-Sanchez, E., Non-destructive techniques based on eddy current testing, Sensors, 3 (2011) 2525-2565.
- [7] Harzallah, S., Chabaat, M., Nondestructive technique for the determination of cracks parameters by eddy current in differential mode, Journal of Applied Mechanics & Materials, 532 (2014) 81-89.
- [8] Harzallah, S., Chabaat, M., Benissad, S., Formulation for stress intensity factors and J-integral calculation by eddy current testing, International Journal of Key Engineering Materials, 660 (2015) 225-230.
- [9] Harzallah, S., Chabaat, M., Benissad, S., Inverse problems using neural networks for cracks characterization in materials, International Journal of Key Engineering Materials, 660 (2015) 361-365.
- [10] Harzallah, S., Chabaat, M., Eddy current sensor modeling for the nondestructive evaluation of stress intensity factor, Journal AASRIProcedia, Elsevier Ltd., 9 (2014) 57–63.
- [11] Harzallah, S., Chabaat, M., Bin Muhammad, B.F., Eddy current modeling by finite element method for evaluation of mechanical properties of the structure cracked in absolute probe, AIP Conference Proceedings, 1637(1) (2014) 1416.
- [12] Harzallah, S., Chabaat, M., Bin Muhammad, B.F., Non destructive technique for cracks detection by an eddy current in differential mode for steel frames, AIP Conf. Proc., 1637 (2014) 1406.
- [13] Chabane, K., Harzallah, S., Chabaat, M., 3D eddy current testing by FEM for detection of cracks in materials, International Journal of Key Engineering Materials, 703 (2016) 349.